Journal of Energy Storage 64 (2023) 107229

Contents lists available at ScienceDirect

Journal of Energy Storage

journal homepage: www.elsevier.com/locate/est

Research papers

Effect of relative permeability hysteresis on reservoir simulation of underground hydrogen storage in an offshore aquifer

Maksim Lysyy *, Martin A. Fernø, Geir Ersland

Department of Physics and Technology, University of Bergen, Allegaten 55, 5007 Bergen, Norway

ARTICLE INFO

Keywords:
Underground hydrogen storage
Natural gas storage
Reservoir simulation
Storage capacity
Cyclic injections
Hysteresis

ABSTRACT

Underground hydrogen storage (UHS) in porous media is proposed to balance seasonal fluctuations between demand and supply in an emerging hydrogen economy. Despite increasing focus on the topic worldwide, the understanding of hydrogen flow in porous media is still not adequate. In particular, relative permeability hysteresis and its impact on the storage performance require detailed investigations due to the cyclic nature of H_2 injection and withdrawal. We focus our analysis on reservoir simulation of an offshore aquifer setting, where we use history matched relative permeability to study the effect of hysteresis and gas type on the storage efficiency. We find that omission of relative permeability hysteresis overestimates the annual working gas capacity by 34 % and the recovered hydrogen volume by 85 %. The UHS performance is similar to natural gas storage when using hysteretic hydrogen relative permeability. Nitrogen relative permeability can be used to model the UHS when hysteresis is ignored, but at the cost of the accuracy of the bottom-hole pressure predictions. Our results advance the understanding of the UHS reservoir modeling approaches.

1. Introduction

Hydrogen (H_2) will play a vital role in the future net-zero energy mix and its industrial scale-up will require a range of storage solutions in all dimensions and time scales. Underground H_2 storage (UHS) has been proposed as one storage option which can account for seasonal and regional variations in demand and supply [1]. The H_2 storage demand in Europe in 2050 is expected to be in the range of 63–180 billion Sm^3 (standard cubic meter) under the assumption of 780–2251 TWh total demand [2] and 24 % storage capacity [3]. Relevant underground storage formations include salt caverns, depleted hydrocarbon fields and aquifers [4] as well as more unconventional storage sites such as coal seams and basaltic rocks [5,6]. Salt caverns can accommodate smaller H_2 volumes to meet short-term storage needs, whereas porous reservoirs (i.e. depleted fields and aquifers) can be suitable for larger H_2 volumes in the long-term. Most potential storage sites are considered onshore, but offshore H_2 storage in the North Sea is attractive with regards to existing infrastructure and a growing offshore wind industry [7]. Water electrolysis can use wind-based excess electricity to produce H_2 that can be stored underground for later use.

Technically, the UHS is similar to natural gas storage (UGS) with gas injection at peak supply, followed by gas withdrawal at peak demand in repeatable annual cycles. To maintain a stable pressure support during withdrawal, cushion gas is required to remain in the reservoir while working gas is cyclically injected and withdrawn [1]. The cushion and working gases can be the same or differ in its type. Pure H_2 has never been stored in porous reservoirs at commercial scale, with town gas storage in aquifers in the 1970s [8,9] and two recent pilot tests of H_2 blends in depleted gas fields [10,11].

Despite technical similarities, low H_2 density and viscosity coupled with high biogeochemical activity hampers direct knowledge transfer [4,12]. H_2 wettability, biogeochemical interactions and reservoir simulations are currently dominating the research literature. It was found out that H_2 is a non-wetting phase in sandstones with pure quartz surfaces and is less wetting than CO_2 [13–16]. An empirical equation of H_2-brine interfacial tension was derived from experimental measurements under a range of pressure, temperature and brine salinity conditions [17]. Evaluation of caprock interfacial tension and wettability for H_2 storage showed that caprock integrity decreased with increasing pressure, temperature, organic acid concentration and total organic content [18,19]. H_2 geochemical reactivity was suppressed in calcite- and anhydrite-free sandstones [20–22]. Reservoir simulations showed that the UHS performed differently than CH_4 and CO_2 storage when comparing gas containment and working capacity [23].

* Corresponding author.
E-mail address: Maksim.Lysyy@uib.no (M. Lysyy).

https://doi.org/10.1016/j.est.2023.107229
Received 30 January 2023; Received in revised form 20 March 2023; Accepted 22 March 2023
Available online 30 March 2023

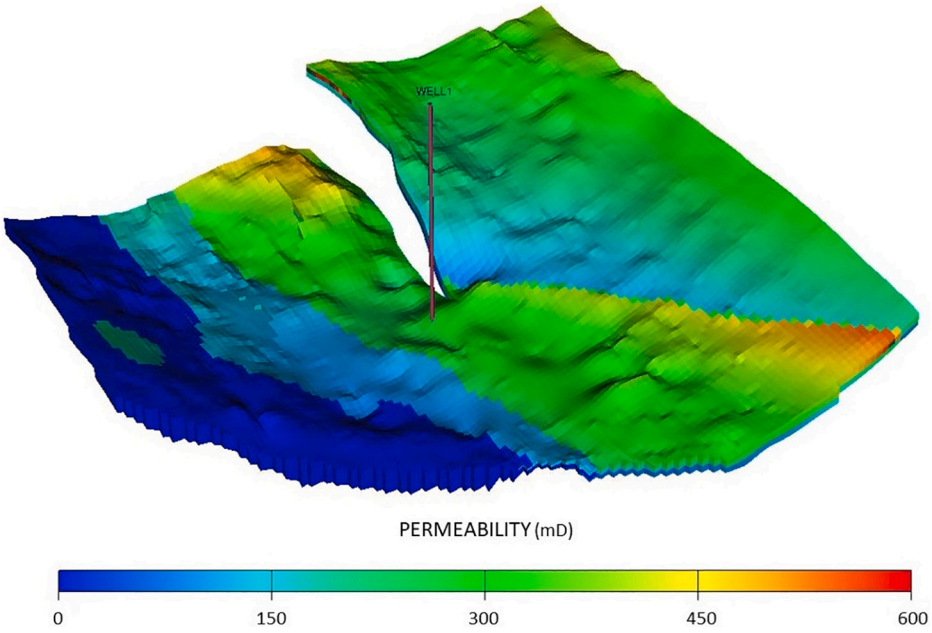

Fig. 1. A sector model of the Johansen formation with the well location and horizontal permeability distribution. The lateral extent of the sector model is around 50 km × 50 km, with the average grid size of 500 m × 500 m × 20 m. Shale layers above the Johansen formation are not shown. The vertical distance is 10 times exaggerated.

Reservoir simulation is a valuable and time efficient tool for decision making and predicting future storage performance under different reservoir management strategies. The UHS reservoir simulation studies mostly focused on feasible strategies to estimate the ultimate H_2 recovery and the impact of cushion gas. The maximum recovery factor of 78 % was achieved for single cycles in a saline aquifer, with the highest H_2 saturation in the near-well area and the reservoir top [24]. H_2 storage in a depleted oil and gas field showed that the gas zone was the most suitable target with a final recovery factor of 87 %, that was reduced to 49 % in the water zone [25]. The cushion-to-working gas ratio varied between 0.15 and 1.5 in a saline aquifer, being the lowest in deeper reservoirs with higher permeability [26]. Among different types of cushion gases: CH_4, N_2 and CO_2, the highest H_2 recovery factor (90 %) was achieved with CH_4 in a depleted oil reservoir [27], whereas N_2 was the most effective cushion gas in a partially depleted gas condensate reservoir with the H_2 recovery factor of 98 % [28]. Screening criteria for site selection were proposed based on the reservoir pressure, dipping angle, storage depth, geothermal gradient and permeability and porosity range [29].

Most UHS studies implemented nonhysteretic relative permeability in reservoir models, not specifically measured for H_2. Despite being more reliable than analytical methods, the reservoir models require real field and/or experimental data for more accurate predictions. It is still debated whether a proxy gas can be used to accurately model H_2 behavior. The gas-water injection experiments in sandstone core samples showed that N_2 is a poor proxy gas for H_2 [30,31], or it should be used with care [32]. In contrast, the opposite conclusion was drawn from another study stating that N_2 can be used as a proxy gas [33]. On the other hand, cyclic H_2 injection and withdrawal will result in reversable drainage and imbibition processes in the reservoir, indicating that relative permeability hysteresis must be considered in reservoir simulations. Measurements of H_2-H_2O drainage and imbibition relative permeability confirmed strong hysteresis both for H_2 and H_2O [32,34].

Reservoir simulation studies on the impact of H_2-H_2O relative permeability hysteresis are scarce. Hysteresis was considered in an aquifer H_2 storage study [35] where relative permeability and capillary pressure were derived from an analytical van Genuchten–Mualem model aimed to represent a typical gas-H_2O system in a sandstone. The relative permeability model resulted in a pronounced gas hysteresis, whereas H_2O showed a minor difference between drainage and imbibition. The impact of hysteresis on H_2 storage efficiency was not evaluated as the model did not include a nonhysteretic case for comparison. One of the first attempts to study the impact of hysteresis on H_2 storage was performed in a synthetic aquifer reservoir [36]. The authors used the experimentally measured drainage H_2-H_2O relative permeability [37] and the Killough model [38] to construct imbibition H_2 relative permeability, but hysteresis in H_2O relative permeability and capillary pressure was neglected. Another study of aquifer storage implemented both H_2 and H_2O relative permeability hysteresis [39], derived from pore scale modeling without experimental support [40]. A more recent study [41] implemented the measured hysteretic H_2-H_2O relative permeability [34], and performed an analytical extrapolation beyond experimental endpoints. No history matching of experimental pressure and production data was performed to confirm the analytical extrapolation and capillary pressure hysteresis was neglected. For imbibition H_2O relative permeability, they could not find a reliable analytical model and used tabulated experimental data instead.

The abovementioned studies agreed that the absence of relative permeability hysteresis overestimated the H_2 recovery factor but disagreed in terms of H_2O production. The performance of H_2 and CO_2 storage were significantly different [39], and CO_2 relative permeability cannot be used as a proxy to model the UHS [41]. Note that impact of hysteresis has been extensively investigated for CO_2 storage, indicating that hysteresis is necessary for more accurate modeling approaches [42–45]. Experiences from CO_2 hysteresis studies are not directly applicable for H_2 storage due to the absence of CO_2 withdrawal stage.

In this paper, we use reservoir simulation to study the UHS in an offshore aquifer. We implement the measured hysteretic H_2-H_2O relative permeability and capillary pressure with numerical extrapolation from history matching of experimental production and pressure data [32], thus being a more accurate input for reservoir simulations. The Johansen sandstone formation was selected as a storage site with a real geological model built for CO_2 storage studies on the Norwegian continental shelf [46]. We examine the impact of hysteresis and a proxy gas relative permeability on the UHS and compare the results with CH_4 storage. Our findings emphasize the importance of relative permeability

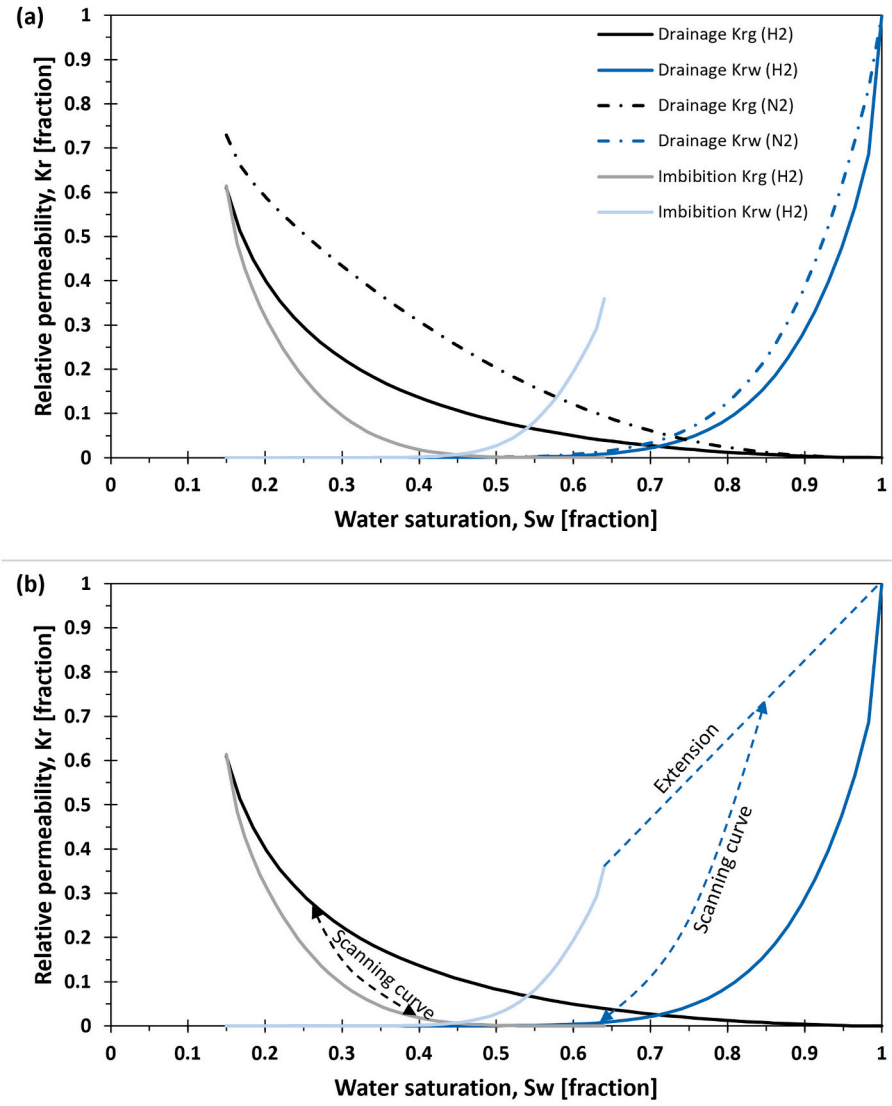

Fig. 2. Input relative permeability curves and hysteresis model used in the simulations. (a) H_2-H_2O (solid curves) and N_2-H_2O (dashed curves) relative permeabilities were directly taken from the literature dataset, derived from experimental measurements and numerical history matching [32]. The drainage H_2 (K_{rg}) and H_2O (K_{rw}) curves are represented by black and dark blue colour, respectively; whereas the imbibition K_{rg} and K_{rw} are denoted by grey and light blue, respectively. For drainage, the endpoint K^*_{rg} at irreducible H_2O saturation of 0.15 are equal to 0.61 and 0.73 for H_2 and N_2, respectively. For imbibition, the endpoint K^*_{rw} at residual H_2 saturation of 0.36 is equal to 0.36. (b) Killough hysteresis model applied to input H_2-H_2O relative permeability. The dashed curves with arrows represent typical scanning curves starting at arbitrary points. (For interpretation of the references to colour in this figure legend, the reader is referred to the web version of this article.)

hysteresis for accurate modeling of underground H_2 storage in reservoirs.

2. Numerical methods

2.1. The Johansen simulation model

The Johansen formation on the Norwegian continental shelf was selected as a storage site in our study. We used an open-license geological sector model with heterogenous porosity and horizontal permeability distribution of 0.1–0.29 (average 0.15) and 0.01–875 (average 97) mD, respectively [46]. The vertical permeability was set to 10 % of the horizontal one. The sector model was discretized into 100 × 100 × 11 grid cells with an average grid size of 500 m × 500 m × 20 m (Fig. 1). The sandstone reservoir was represented by five grid layers, vertically connected to five shale layers above and one shale layer below the reservoir. The model was constructed with a non-zero dipping angle and five faults with the transmissibility multipliers of 0.1. A more detailed description of the Johansen formation and its geological model can be found elsewhere [47].

We used a commercial black-oil ECLIPSE reservoir simulator to construct a dynamic model of the Johansen formation. The model was governed by Darcy's law and mass conservation and contained two components: gas and water. Diffusion, dissolution and biogeochemical reactions were not included to focus on the UHS hydrodynamics. The model was initiated with no-flow boundary conditions and pressure of 313.1 bar at 3100 m true vertical depth. The gas and water densities and viscosities were extracted from an open-source database for a pressure range of 50–500 bar and reservoir temperature of 94 °C [48]. Relative permeability and capillary pressure were directly taken from the literature H_2 dataset, derived from history matched experimental measurements in a sandstone with permeability of 107 mD [32]. The rock type and its permeability are comparable to the Johansen sandstone reservoir with the average model permeability of 97 mD, making the literature dataset reliable for our H_2 storage study. Both nonhysteretic and hysteretic relative permeabilities and capillary pressures were considered, described next.

2.2. Relative permeability hysteresis model

Drainage relative permeability and capillary pressure functions were implemented in a nonhysteretic case, where two different sets of relative permeabilities were tested: H_2-H_2O and N_2-H_2O (Fig. 2a). In a hysteretic case, drainage and imbibition relative permeability and capillary

Table 1
Summary results of H_2 and CH_4 storage schemes with different relative permeability (K_r) input.

Gas type	Input K_r	Gas withdrawn [Million Sm^3]					Gas recovery factor	
		1st cycle	2nd cycle	3rd cycle	4th cycle	5th cycle	1st cycle	Final
H_2	Drainage H_2-H_2O	540	540	540	540	1560	16 %	68 %
H_2	Drainage N_2-H_2O	540	540	540	540	1550	16 %	68 %
H_2	Hysteretic H_2-H_2O	451	390	388	393	391	14 %	37 %
CH_4	Hysteretic H_2-H_2O	436	378	376	380	380	13 %	37 %

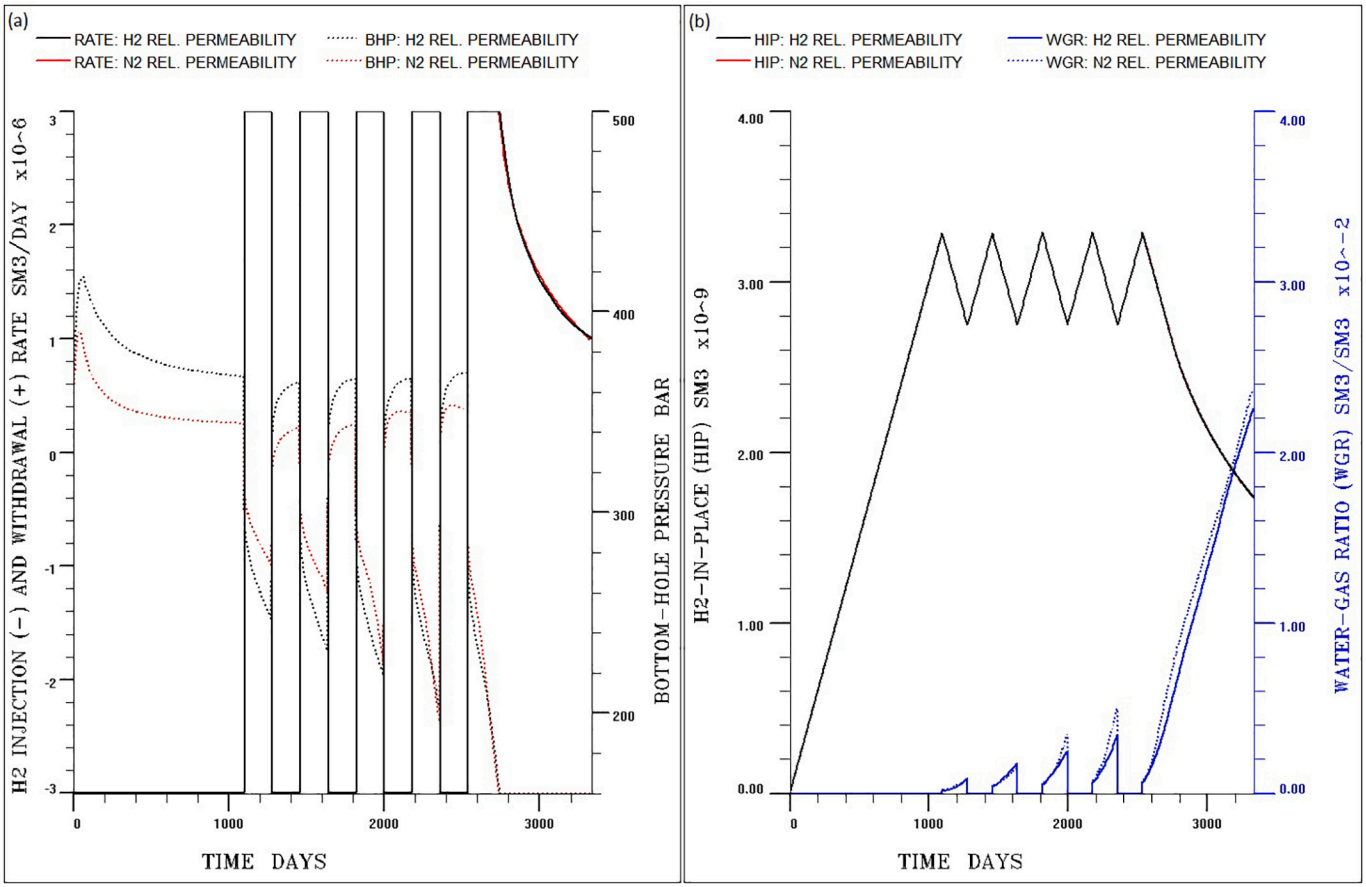

Fig. 3. Nonhysteretic case of H_2 storage with two different simulation inputs: H_2 and N_2 relative permeabilities. (a) H_2 injection (negative values) and withdrawal (positive values, solid curves on the primary x-axis) rates and the bottom-hole pressure (BHP, dashed curves on the secondary x-axis). The first injection period lasted for 1095 days, and the prolonged fifth withdrawal period began after 2538 days. The constant injection/withdrawal rates of 3 million Sm^3/d were maintained until the prolonged fifth withdrawal period, characterized by a rate reduction due to a BHP limit of 180 bar. (b) H_2 volume in place (HIP, black and red curves on the primary x-axis) and water-gas ratio (WGR, blue curves on the secondary x-axis). The HIP remained in the same range during the cyclic injection and withdrawal, whereas the WGR increased with the increasing number of cycles. The H_2 and N_2 relative permeabilities showed similar results, except for the BHP development. (For interpretation of the references to colour in this figure legend, the reader is referred to the web version of this article.)

pressure were applied for both gas and water using the Killough hysteresis model [38]. The hysteresis model implies that relative permeability functions follow a scanning curve when drainage or imbibition processes are reversed (Fig. 2b). The same scanning curve is applied for both drainage and imbibition when the injection process is reversed at any point on the scanning curve. Non-wetting phase (H_2) scanning curves are calculated based on an interpolative method that requires Land trapping model [49] and bounding drainage and imbibition curves as input. In the absence of experimental bounding data, the scanning curves can be estimated using a parametric interpolation method, which requires an input free parameter. In our case, the ECLIPSE simulator generated scanning curves from experimental drainage and imbibition data [32]. Wetting phase (H_2O) scanning curves additionally require a free parameter (set to 1 in our model), even if experimental bounding curves are given. The H_2O scanning curve may deviate beyond a region enclosed by the drainage and imbibition curves if the imbibition curve initial gradient is small. To keep H_2O scanning curve inside the region of drainage and imbibition curves, the ECLIPSE simulator runs a correction scheme based on the reduced portion of the imbibition curve.

2.3. Storage scenarios

We evaluated four storage scenarios with both nonhysteretic and hysteretic relative permeability curves (Table 1). In the nonhysteretic cases, we examined the effect of relative permeability on the H_2 storage performance by comparing two different inputs: drainage H_2-H_2O and N_2-H_2O relative permeabilities. In the hysteretic cases, the same set of drainage and imbibition H_2-H_2O relative permeabilities was

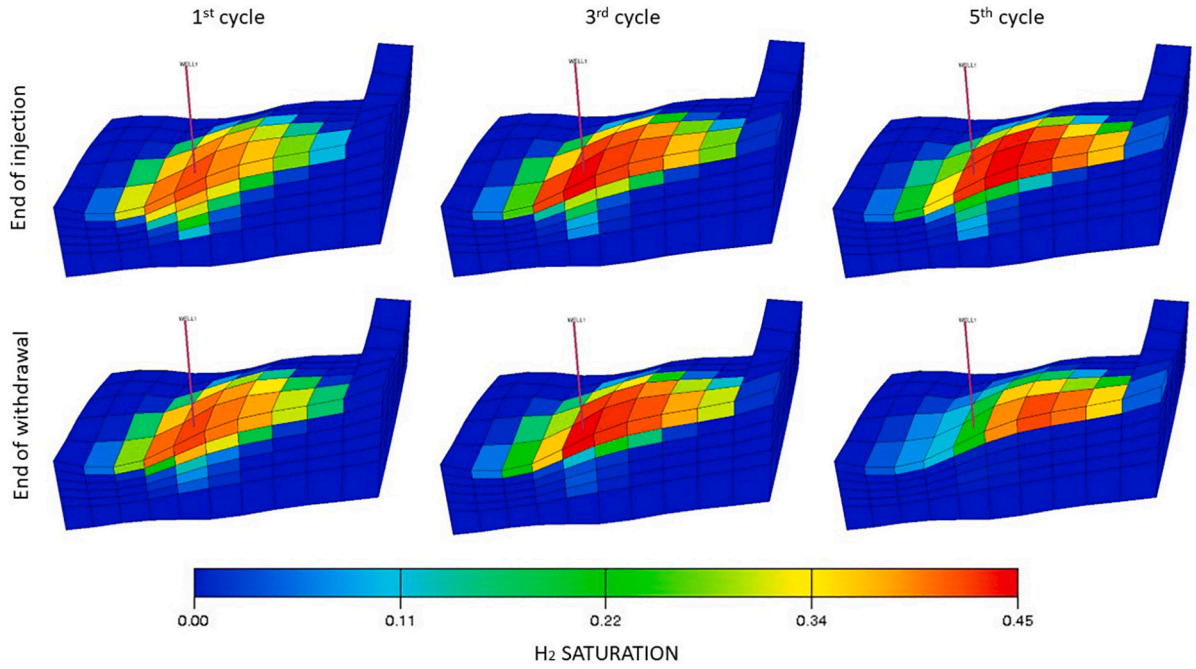

Fig. 4. Vertical slice of the 3D simulation grid part showing H_2 distribution by the end of injection (top) and by the end of withdrawal (bottom) after the 1st, 3rd and 5th cycles in the nonhysteretic case. The H_2 plume formed a cone-like shape with a stable lateral extent which contracted vertically during withdrawal, with the highest H_2 saturation at the top well perforation. Vertical distance is 10-times exaggerated.

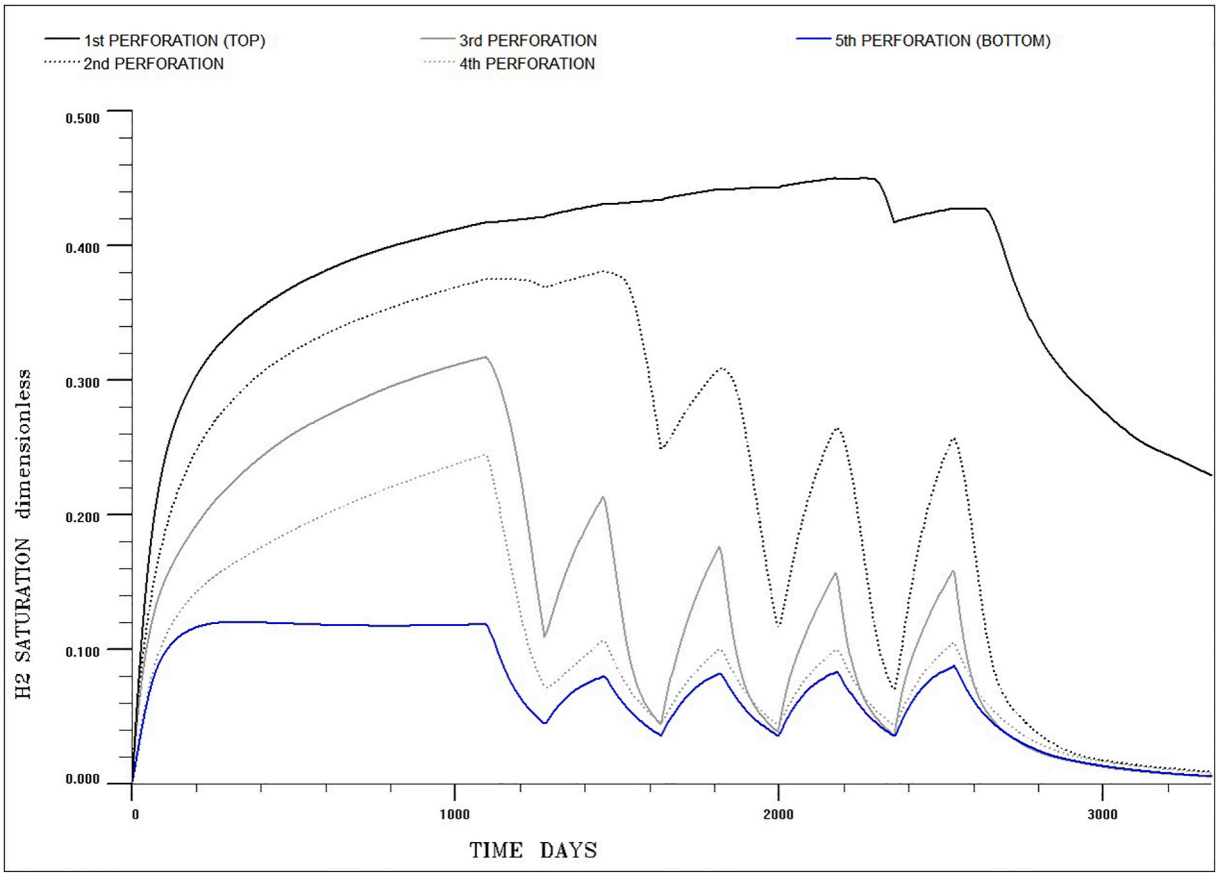

Fig. 5. H_2 saturation in the well perforations, numbered from top (1st) to bottom (5th). The H_2 saturation increased with increasing number of cycles in the 1st perforation but decreased in the 2nd and 3rd perforations due to water upconing.

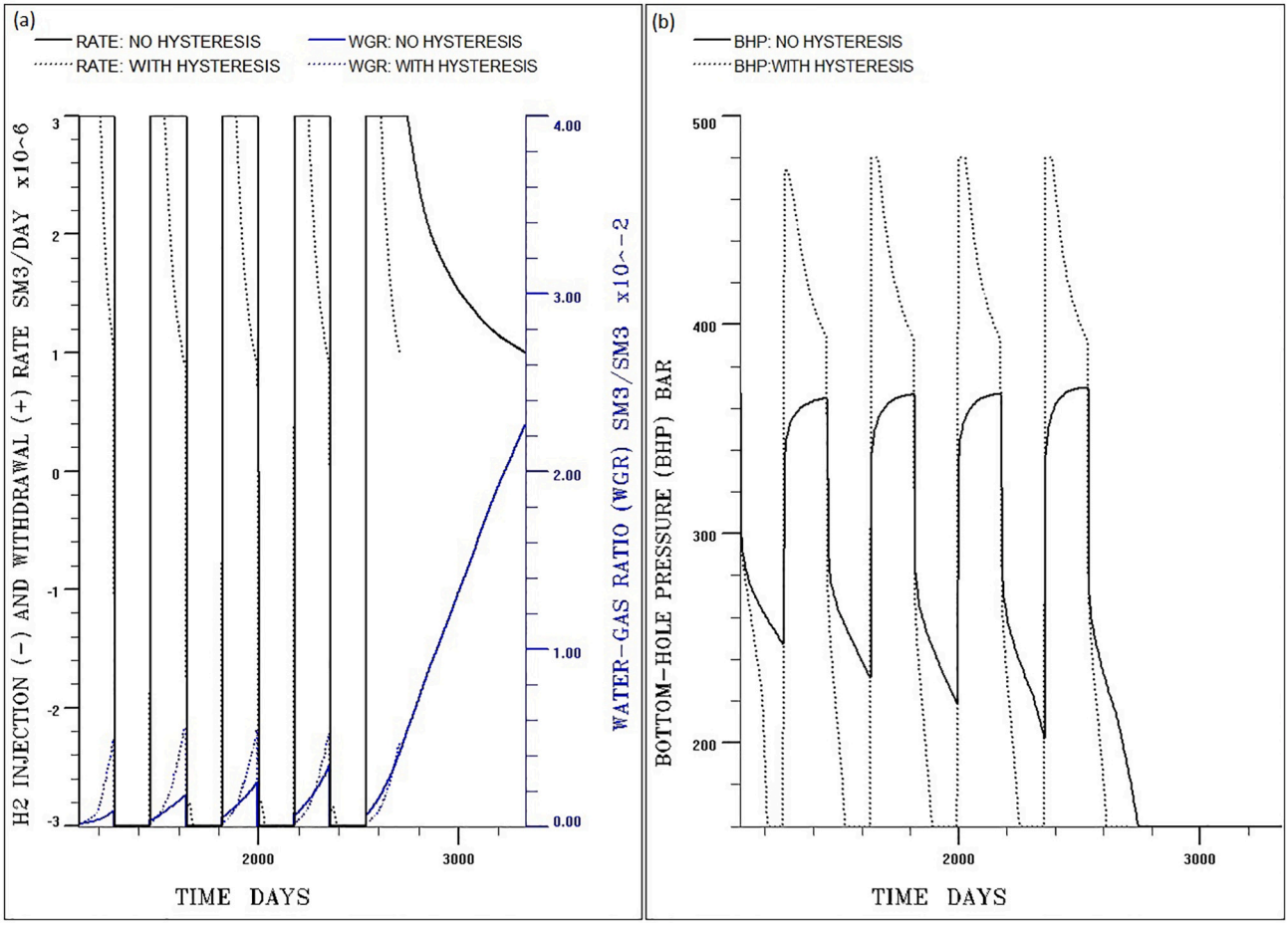

Fig. 6. Effect of relative permeability hysteresis on the storage performance. (a) H_2 injection (negative values) and withdrawal (positive values, black curves on the primary x-axis) rates and water-gas ratio (WGR, blue curves on the secondary x-axis). (b) Bottom-hole pressure (BHP). The hysteresis resulted in lower withdrawal and injection rates caused by the lower and upper BHP limits, respectively. The WGR increased and remained nearly constant in the hysteretic case. (For interpretation of the references to colour in this figure legend, the reader is referred to the web version of this article.)

implemented to compare the H_2 and CH_4 storage.

All storage scenarios followed the same operation scheme: Five injection-withdrawal cycles at the rate of 3 million Sm^3/d, with H_2 acting as both cushion and working gas. The first cycle started with a 36-month long initial filling with gas, followed by a six-month withdrawal period. The three subsequent cycles were repeated annually, with equally long injection and withdrawal periods of six months. The fifth cycle consisted of a six-month injection period, followed by a prolonged withdrawal period until the economic limit of 1 million Sm^3/d was reached [25]. A single vertical well for injection and withdrawal was placed in the center of the reservoir model through the five grid blocks where the permeability and porosity ranged between 74 and 278 mD and 0.17–0.21, respectively. The well operation was controlled by the bottom-hole pressure (BHP), constrained to 480 and 160 bar during injection and withdrawal, respectively. The BHP constrains were equal to ±50 % of the initial reservoir pressure where the upper BHP limit was below the typical fracture pressure on the Norwegian continental shelf [50]. When the BHP limits were reached, the injection/withdrawal rates were reduced to maintain constant BHP.

3. Results and discussion

3.1. Maximum working gas capacity and recovery factor

The first injection period maintained a pre-defined H_2 injection rate of 3 million Sm^3/d, but with a nonmonotonic BHP (Fig. 3a). An initial sharp increase in BHP by 110 bar from the initial reservoir pressure reversed to a gradually declining trend as the H_2 plume expanded away from the injector. The withdrawal periods were characterized by an initial sharp decrease in BHP, followed by a more gradual trend. The endpoint BHP decreased with an increasing number of cycles, due to increasing water production with a resulting increase in the bottom-hole saturation of incompressible water (Fig. 3b).

The maximum working gas capacity was 540 million Sm^3 (~1.6 TWh) in all six-month withdrawal periods, achieved with nonhysteretic H_2-H_2O relative permeability (Table 1). The working gas capacity was equivalent to 16 % of the total H_2 volume injected during the first injection period and corresponded to 0.9 % of the predicted lower-end H_2 storage demand in Europe in 2050 [3]. The working-to-total gas volume ratio was consistent with the reported literature range of ~15–30 % when using H_2 cushion gas in aquifer storage [23–25,36]. Note that the working gas capacity increases if H_2 is replaced by other cushion gases, albeit with a decrease in H_2 fraction in the withdrawn gas mixture [25,27,36].

The maximum final H_2 recovery factor was 68 % by the end of the prolonged fifth withdrawal period which lasted for 795 days until an economic limit of 1 million Sm^3/d was reached (Table 1, Fig. 3a). Constant withdrawal rate of 3 million Sm^3/d was maintained for 207 days, followed by a declining rate due to the lower BHP limit. Comparable recovery factors (69–75 %) were reported for aquifer storage where the BHP upper limit was set to ≥50 % of the initial reservoir pressure [36,51]. In contrast, a significantly lower recovery factor (49

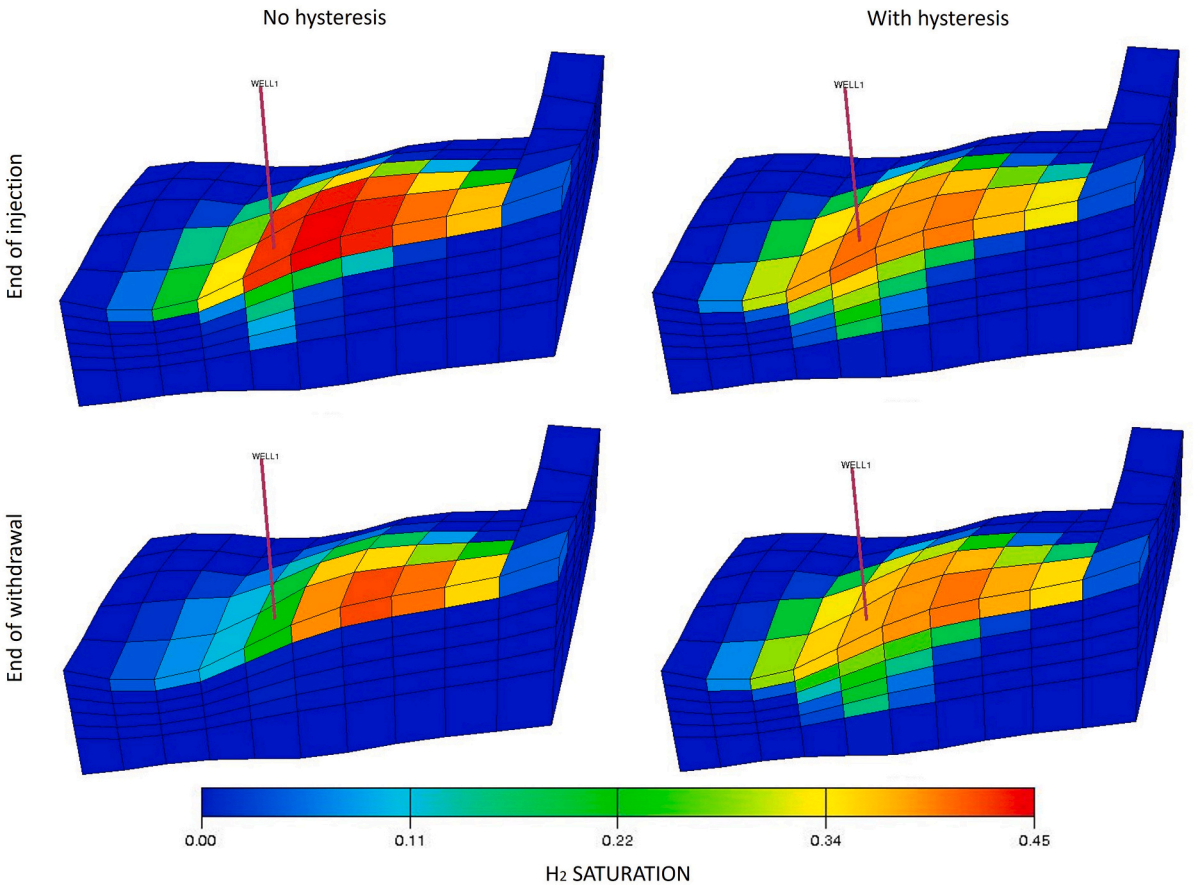

Fig. 7. Effect of relative permeability hysteresis on the H_2 distribution by the end of injection (top) and by the end of withdrawal (bottom) after the 5th cycle in the nonhysteretic (left) and hysteretic cases (right). After injection, the H_2 saturation was more concentrated in the near-well area in the nonhysteretic case due to decreased residual trapping. After withdrawal, the H_2 saturation accumulated in all perforated layers in the hysteretic case due to less H_2 volume withdrawn.

%) was estimated for the isolated water zone in a depleted hydrocarbon field because the upper BHP limit was set to the initial reservoir pressure [25]. Discrepancies in the recovery factors show that the BHP constraints are among the crucial parameters affecting the H_2 storage efficiency.

3.1.1. *Effect of proxy gas relative permeability*

N_2 relative permeability was evaluated as the simulation input and showed no significant impact on working gas capacity and recovery (Table 1, Fig. 3). An initial 10 % decrease in BHP during the first injection period diminished with an increasing number of cycles to a 5 % difference by the end of the fifth injection period. The results suggest that N_2 relative permeability can be used as proxy in reservoir simulations in the absence of H_2 relative permeability data. However, a mismatch between the measured and simulated BHP may be expected during real storage projects. For comparison, CO_2 relative permeability failed to accurately model the UHS [41].

3.1.2. *Hydrogen plume dynamics*

The H_2 plume developed a cone-like shape in vertical direction, governed by gravitational effects (Fig. 4). The maximum H_2 saturation was established in the top perforation (S_g = 0.42), with a gradually decreasing H_2 saturation toward the plume boundaries (minimum S_g = 0.06). The withdrawal periods were characterized by an upward shrinking of the H_2 plume, leading to water upconing in the well. No lateral movement of the H_2 plume was observed because the injected and withdrawn H_2 volumes were equal for all six-month periods. A stable lateral distribution is beneficial for H_2 storage because it minimizes the risk of leakage at the reservoir boundaries. The observed H_2 plume dynamics was consistent with the literature [24,35,36,51].

The H_2 saturation in the top perforation increased with an increasing number of cycles, from 0.42 to 0.45 by the end of the first and fifth injection periods, respectively (Fig. 5). In contrast, the H_2 saturation decreased in the second and third perforations, whereas this effect was suppressed in the lower perforations. This demonstrates that water upconing is more pronounced in the middle part of the well. The final H_2 distribution by the end of the prolonged fifth withdrawal period accumulated at the reservoir top.

3.2. *Effect of relative permeability hysteresis*

Implementation of relative permeability hysteresis reduced the working gas capacity and final recovery factor, compared with the nonhysteretic case (Table 1). The working gas capacity after the first cycle decreased from 540 to 451 million Sm^3, with a further reduction to 393 million Sm^3 after the fifth cycle. The duration of the prolonged fifth withdrawal period was shortened by 627 days, yielding a significant reduction in the final H_2 recovery factor from 68 % to 37 % (Table 1). The reduction in the working gas capacity and recovery factor was attributed to reaching the lower BHP during withdrawal, leading to a reduction in the withdrawal rates to maintain constant pressure (Fig. 6). The BHP decrease was governed by the inflow performance relationship in Eclipse reservoir simulator: $Q_g = T_w \bullet M_g \bullet (p_{grid} - p_{BHP} - p_{head})$, where Q_g is the H_2 withdrawal rate, T_w is the grid connection transmissibility factor, M_g is the H_2 mobility, p_{grid} is the grid connection pressure, p_{BHP} is the BHP, and p_{head} is the pressure head between the grid connection and bottom hole. The BHP must reduce to maintain a constant H_2 withdrawal rate at the reduced H_2 mobility caused by lower H_2 relative

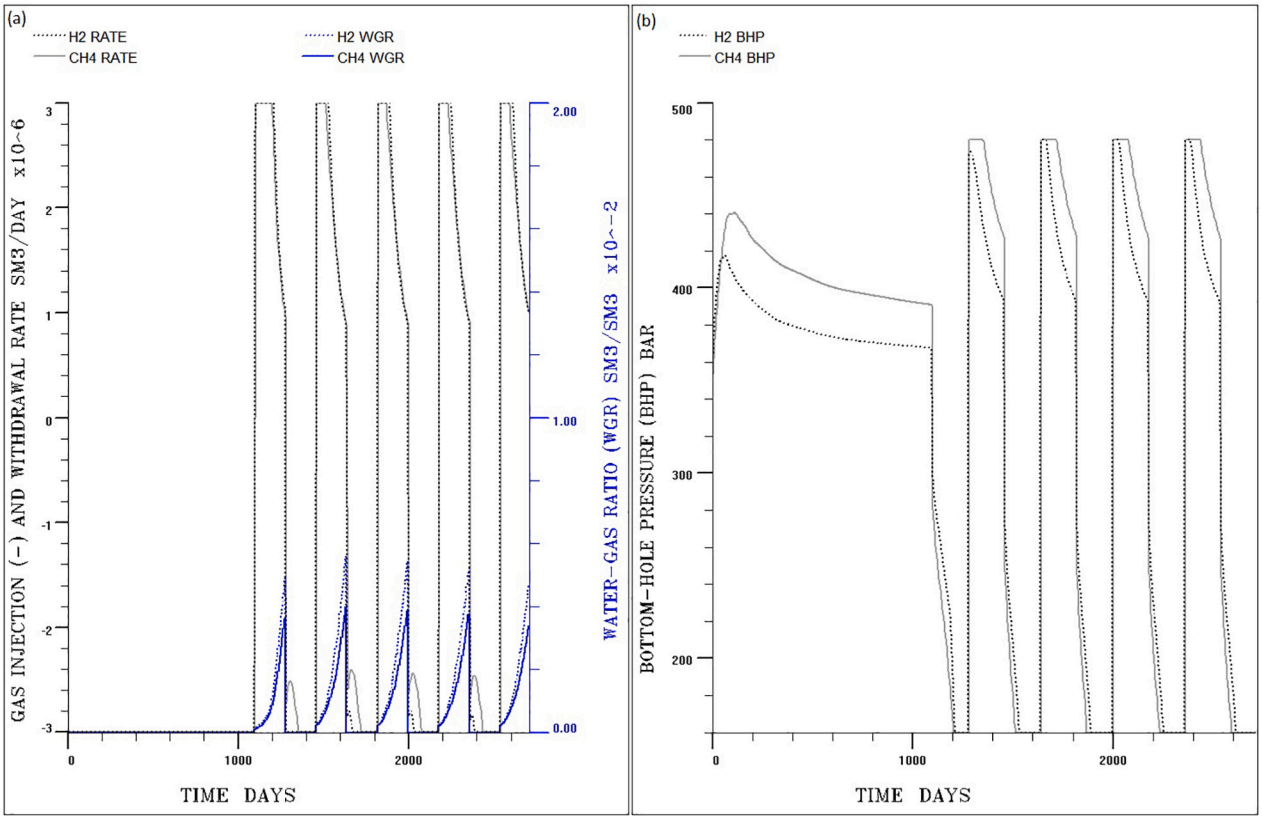

Fig. 8. Effect of gas type on the storage performance using the hysteretic relative permeability. (a) Gas injection (negative values) and withdrawal rates (positive values, black curves on the primary x-axis) and water-gas ratio (WGR, blue curves on the secondary x-axis). (b) Bottom-hole pressure (BHP). The injection and withdrawal rates were similar, whereas CH_4 storage resulted in lower WGR and higher injection BHP. (For interpretation of the references to colour in this figure legend, the reader is referred to the web version of this article.)

permeability.

A higher BHP during injection (Fig. 6b) was due to the reduced H_2 mobility, requiring higher pressure to maintain the same injection rate as in the nonhysteretic case. The upper BHP limit was reached in the third-fifth injection periods, reducing the H_2 injection rates to 2.8 million Sm^3/day before gradually returning to 3 million Sm^3/day after the first 25 days. The water-gas ratio (Fig. 6a) was nearly constant by the end of withdrawal periods, but about six times higher than in the non-hysteretic case in the first cycle, diminishing to a 1.5 times difference in the fourth cycle.

Reduction in the working gas capacity and recovery factor due to hysteresis agreed with other reservoir simulation studies of H_2 storage in aquifers [36,39]. The authors reported a 15 % reduction in the working gas capacity after the first cycle, but the difference with the non-hysteretic case decreased with increasing number of cycles. The final recovery factor was reduced by 5 percentage points after the fifth cycle, from 69.1 % to 64.1 % [36] and from 31 % to 26 % [39]. The reduction in storage efficiency in the hysteretic case was explained by the increased residual trapping, making the disconnected H_2 phase more difficult to mobilize. A higher reduction in the H_2 recovery factor was reported after the 10th cycle, from 98 % to 82–84 % depending on the hysteresis model [41]. Low recovery factors between 7 % and 36 % and their dependency on the injection rate were reported for a one-cycle storage scheme with a caprock present [35]. This was likely caused by a short duration of the withdrawal stage (one year) compared to the injection stage (three years) and hysteresis, but a direct comparison with the nonhysteretic case was missing.

The increased water-gas ratio due to hysteresis was consistent with one study [41]. In contrast, two other studies reported a decreased water-gas ratio [36,39], likely caused by lower water relative permeability and/or inclusion of a shut-in period. Lower imbibition water relative permeability at the endpoint (<0.20) than in our study (0.36) led to lower water mobility, whereas a shut-in period contributed to a higher H_2 concentration in the near-well area prior to withdrawal. Discrepancies between different studies imply that there is no universal rule regarding the water production handling, which seems to depend on input parameters and operational conditions. Detailed pre-screening with reservoir simulations is therefore required when planning real storage projects.

The H_2 plume dynamics was comparable to the nonhysteretic case, with a vertical contraction during withdrawal and a stable lateral extent (Fig. 7). However, in the nonhysteretic case the vertical H_2 distribution was more concentrated in the well perforations, with 0.03 higher H_2 saturation in the top perforation after the fifth injection period, compared to the hysteretic case. This was because of the decreased residual trapping, enabling more H_2 to mobilize and accumulate in the near-well area. In the hysteretic case, the unrecovered H_2 after the prolonged fifth withdrawal period accumulated not only in the top layer, but also in the lower layers in a cone-like shape.

3.3. *Effect of gas type: H_2 vs CH_4 storage*

We used the hysteretic H_2 relative permeability to compare H_2 and CH_4 storage schemes. The working gas capacity and final recovery factors were comparable (Table 1), but with differences in the BHP and water-gas ratio (Fig. 8). The CH_4 injection resulted in higher BHP and longer injection duration at the BHP upper limit (Fig. 8b), leading to smaller injected CH_4 volumes (Fig. 8a). Higher BHP raises the operating costs, and is therefore disadvantageous from an economic perspective [44]. The water-gas ratio by the end of every cycle was on average 28 %

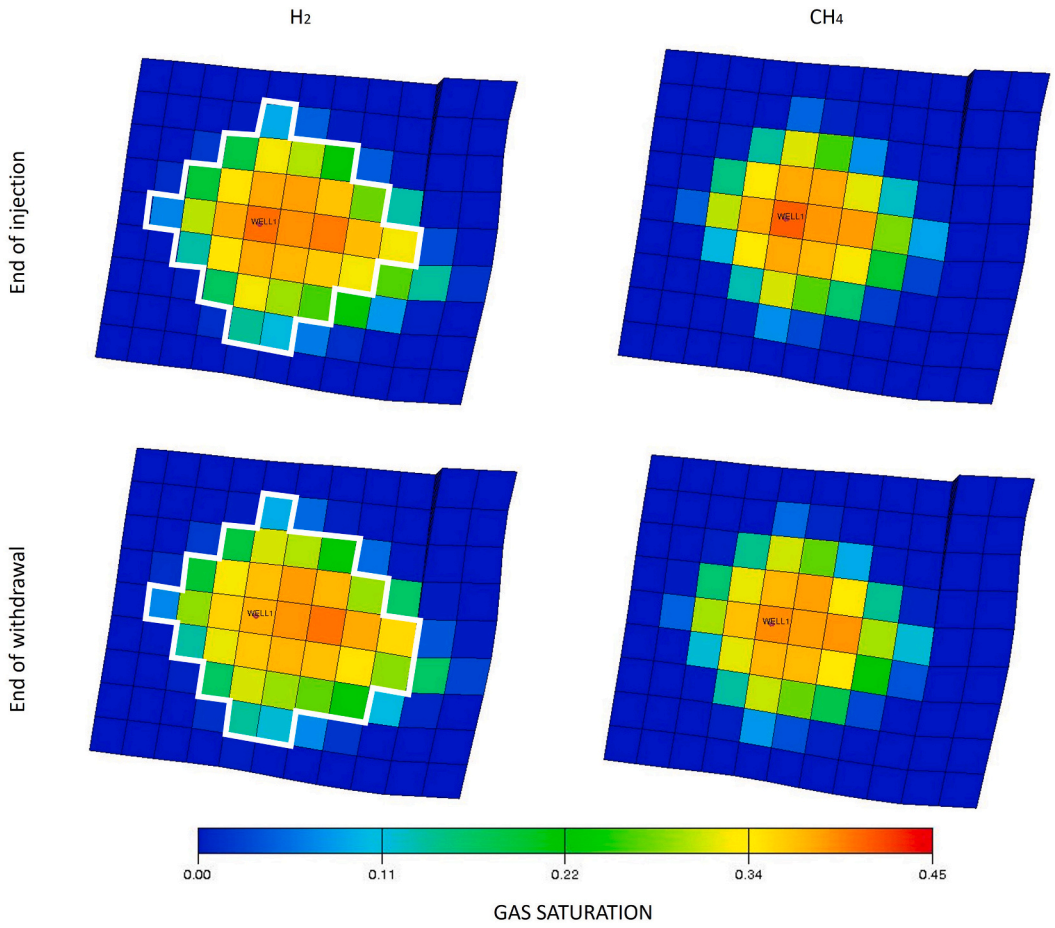

Fig. 9. Effect of gas type on its top-view distribution by the end of injection (top) and by the end of withdrawal (bottom) after the 5th cycle for H_2 (left) and CH_4 (right). The CH_4 plume contours are drawn in white on the left images to compare with the H_2 plume. The CH_4 plume shape appeared to be more uniform, with a less lateral spreading on the right boundary.

lower for CH_4 storage, due to a reduced water-gas mobility ratio. The CH_4 plume lateral spreading was ~500 m shorter than the H_2 plume on the right boundary due to the minor reservoir dipping (Fig. 9). CH_4 is less buoyant, thus less subjected to upslip migration.

Our results indicated that H_2 and CH_4 exhibited a similar performance under the examined conditions, contrary to a single available comparison study [23]. The authors reported a 39 % reduction in the maximum working gas capacity for H_2 storage, caused by a higher wellhead pressure and explained by the difference in the gas physical properties. The discrepancies with our results could be due to the presence of reservoir oil in their study. CH_4 developed a partial miscibility with the reservoir oil, resulting in a higher oil production during CH_4 withdrawal compared with H_2. Moreover, the authors observed a significantly larger lateral extent of the H_2 plume compared to CH_4, due to reservoir heterogeneity and an increasing amount of unrecovered H_2 with the increasing number of cycles.

4. Conclusions

We investigated the impact of the measured and history matched relative permeability hysteresis on H_2 storage in an actual aquifer using a black-oil reservoir simulator. Nonhysteretic relative permeability overestimated the working gas capacity and final recovery factor. Implementation of hysteresis reduced the working gas capacity from 540 million Sm^3 (~1.6 TWh) to 388–451 million Sm^3 and final recovery factor from 68 % to 37 %. The H_2 and CH_4 storage showed comparable working gas capacities and recovery factors when using hysteresis, but CH_4 storage yielded lower water production and higher bottom-hole pressure. Drainage N_2 relative permeability can substitute for missing H_2 data, albeit at the decreased reliability of the bottom-hole pressure predictions. Our results imply that relative permeability hysteresis must be considered to avoid an overestimation of the storage performance and that knowledge transfer from CH_4 to H_2 storage is feasible from a hydrodynamic perspective.

CRediT authorship contribution statement

Maksim Lysyy: Conceptualization, Methodology, Investigation, Formal analysis, Writing – original draft. **Martin A. Fernø:** Writing – review & editing, Supervision, Funding acquisition. **Geir Ersland:** Writing – review & editing, Supervision, Funding acquisition.

Declaration of competing interest

The authors declare that they have no known competing financial interests or personal relationships that could have appeared to influence the work reported in this paper.

Data availability

Data will be made available on request.

Acknowledgements

The authors gratefully acknowledge the financial support from the University of Bergen and from the Research Council of Norway under

project *Hydrogen Storage in Subsurface Porous Media—Enabling Transition to Net-Zero Society* (project number 325457) – a part of the Centre for Sustainable Subsurface Resources (project number 331841).

References

[1] P.O. Carden, L. Paterson, Physical, chemical and energy aspects of underground hydrogen storage, Int. J. Hydrog. Energy 4 (6) (1979) 559–569.
[2] H.J. Undertaking, Hydrogen Roadmap Europe: A Sustainable Pathway for the European Energy Transition, 2019.
[3] J. Cihlar, D. Mavins, K. van der Leun, in: Guidehouse (Ed.), Picturing the Value of Underground Gas Storage to the European Hydrogen System, 2021.
[4] N.S. Muhammed, et al., A review on underground hydrogen storage: insight into geological sites, influencing factors and future outlook, Energy Rep. 8 (2022) 461–499.
[5] M. Hosseini, et al., Basalt-H-2-brine wettability at geo-storage conditions: implication for hydrogen storage in basaltic formations, J.Energy Storage (2022) 52.
[6] S. Iglauer, et al., Hydrogen adsorption on sub-bituminous coal: implications for hydrogen geo-storage, Geophys. Res. Lett. 48 (10) (2021).
[7] A. Hassanpouryouzband, et al., Offshore geological storage of hydrogen: is this our best option to achieve net-zero? ACS Energy Lett. 6 (6) (2021) 2181–2186.
[8] M. Panfilov, Underground and pipeline hydrogen storage, in: Compendium of Hydrogen Energy, Woodhead Publishing, 2016.
[9] P. Smigan, et al., Methanogenic bacteria as a key factor involved in changes of town gas stored in an underground reservoir, FEMS Microbiol. Ecol. 73 (3) (1990) 221–224.
[10] A. Pérez, et al., Patagonia wind - hydrogen project: underground storage and methanation, in: 21st World Hydrogen Energy Conference, 2016. Zaragoza, Spain.
[11] RAG, RAG Austria AG - Underground Sun Storage: Final Report Public 13, 2020.
[12] N. Dopffel, S. Jansen, J. Gerritse, Microbial side effects of underground hydrogen storage - knowledge gaps, risks and opportunities for successful implementation, Int. J. Hydrog. Energy 46 (12) (2021) 8594–8606.
[13] M. Ali, et al., Hydrogen wettability of quartz substrates exposed to organic acids; implications for hydrogen geo-storage in sandstone reservoirs, J. Pet. Sci. Eng. 207 (2021).
[14] L. Hashemi, et al., Contact angle measurement for hydrogen/brine/sandstone system using captive-bubble method relevant for underground hydrogen storage, Adv. Water Resour. 154 (2021).
[15] S. Higgs, et al., In-situ hydrogen wettability characterisation for underground hydrogen storage, Int. J. Hydrog. Energy 47 (26) (2022) 13062–13075.
[16] S. Iglauer, M. Ali, A. Keshavarz, Hydrogen wettability of sandstone reservoirs: implications for hydrogen geo-storage, Geophys. Res. Lett. 48 (3) (2021).
[17] M. Hosseini, et al., H-2-brine interfacial tension as a function of salinity, temperature, and pressure; implications for hydrogen geo-storage, J. Pet. Sci. Eng. 213 (2022).
[18] M. Hosseini, et al., Assessment of rock-hydrogen and rock-water interfacial tension in shale, evaporite and basaltic rocks, J.Nat.Gas Sci.Eng. 106 (2022).
[19] M. Hosseini, et al., Capillary sealing efficiency analysis of caprocks: implication for hydrogen geological storage, Energy Fuel 36 (7) (2022) 4065–4075.
[20] Z. Bo, L. Zeng, Y. Chen, Q. Xie, Geochemical reactions-induced hydrogen loss during underground hydrogen storage in sandstone reservoirs, Int. J. Hydrog. Energy 46 (38) (2021) 19998–20009.
[21] S. Flesch, et al., Hydrogen underground storage-petrographic and petrophysical variations in reservoir sandstones from laboratory experiments under simulated reservoir conditions, Int. J. Hydrog. Energy 43 (45) (2018) 20822–20835.
[22] A.E. Yekta, M. Pichavant, P. Audigane, Evaluation of geochemical reactivity of hydrogen in sandstone: application to geological storage, Appl. Geochem. 95 (2018) 182–194.
[23] M. Delshad, et al., Hydrogen storage assessment in depleted oil reservoir and saline aquifer, Energies 15 (21) (2022).
[24] A. Sainz-Garcia, et al., Assessment of feasible strategies for seasonal underground hydrogen storage in a saline aquifer, Int. J. Hydrog. Energy 42 (26) (2017) 16657–16666.
[25] M. Lysyy, M. Ferno, G. Ersland, Seasonal hydrogen storage in a depleted oil and gas field, Int. J. Hydrog. Energy 46 (49) (2021) 25160–25174.
[26] N. Heinemann, et al., Hydrogen storage in saline aquifers: the role of cushion gas for injection and production, Int. J. Hydrog. Energy 46 (79) (2021) 39284–39296.
[27] M. Kanaani, B. Sedaee, M. Asadian-Pakfar, Role of cushion gas on underground hydrogen storage in depleted oil reservoirs, J.Energy Storage (2022) 45.
[28] M. Zamehrian, B. Sedaee, Underground hydrogen storage in a partially depleted gas condensate reservoir: influence of cushion gas, J. Pet. Sci. Eng. (2022) 212.
[29] E.R. Okoroafor, S.D. Saltzer, A.R. Kovscek, Toward underground hydrogen storage in porous media: reservoir engineering insights, Int. J. Hydrog. Energy 47 (79) (2022) 33781–33802.
[30] A. Al-Yaseri, et al., Initial and residual trapping of hydrogen and nitrogen in Fontainebleau sandstone using nuclear magnetic resonance core flooding, Int. J. Hydrog. Energy 47 (53) (2022) 22482–22494.
[31] E.M. Thaysen, et al., Pore-scale imaging of hydrogen displacement and trapping in porous media, Int. J. Hydrog. Energy 48 (8) (2022) 3091–3106.
[32] M. Lysyy, et al., Hydrogen relative permeability hysteresis in underground storage, Geophys. Res. Lett. 49 (17) (2022).
[33] A. Rezaei, et al., Relative permeability of hydrogen and aqueous brines in sandstones and carbonates at reservoir conditions, Geophys. Res. Lett. 49 (12) (2022).
[34] M. Boon, H. Hajibeygi, Experimental characterization of H-2/water multiphase flow in heterogeneous sandstone rock at the core scale relevant for underground hydrogen storage (UHS), Sci. Rep. 12 (1) (2022).
[35] D.S. Mahdi, et al., Hydrogen underground storage efficiency in a heterogeneous sandstone reservoir, Adv.Geo-Energy Res. 5 (4) (2021) 437–443.
[36] R. Ershadnia, et al., Impact of geological and operational conditions on underground hydrogen storage, Int. J. Hydrog. Energy 48 (4) (2022) 1450–1471.
[37] A.E. Yekta, et al., Determination of hydrogen-water relative permeability and capillary pressure in sandstone: application to underground hydrogen injection in sedimentary formations, Transp. Porous Media 122 (2) (2018) 333–356.
[38] J.E. Killough, Reservoir simulation with history-dependent saturation functions, Soc. Pet. Eng. J. 16 (1) (1976) 37–48.
[39] B. Pan, et al., Impacts of relative permeability hysteresis, wettability, and injection/withdrawal schemes on underground hydrogen storage in saline aquifers, Fuel 333 (2023).
[40] L. Hashemi, M. Blunt, H. Hajibeygi, Pore-scale modelling and sensitivity analyses of hydrogen-brine multiphase flow in geological porous media, Sci. Rep. 11 (1) (2021).
[41] Z. Bo, et al., Impact of experimentally measured relative permeability hysteresis on reservoir-scale performance of underground hydrogen storage (UHS), Int. J. Hydrog. Energy (2023), https://doi.org/10.1016/j.ijhydene.2022.12.270.
[42] E.A. A-Khdheeawi, et al., Influence of injection well configuration and rock wettability on CO2 plume behaviour and CO2 trapping capacity in heterogeneous reservoirs, J.Nat.Gas Sci.Eng. 43 (2017) 190–206.
[43] E.A. Al-Khdheeawi, et al., Impact of reservoir wettability and heterogeneity on CO2-plume migration and trapping capacity, Int.J.Greenhouse Gas Control 58 (2017) 142–158.
[44] R. Juanes, et al., Impact of relative permeability hysteresis on geological CO2 storage, Water Resour. Res. 42 (12) (2006).
[45] S. Krevor, et al., Capillary trapping for geologic carbon dioxide storage - from pore scale physics to field scale implications, Int.J.Greenhouse Gas Control 40 (2015) 221–237.
[46] G.T. Eigestad, et al., The Johansen Data Set. https://co2datashare.org/dataset/the-johansen-dataset, 2009.
[47] G.T. Eigestad, et al., Geological modeling and simulation of CO2 injection in the Johansen formation, Comput. Geosci. 13 (4) (2009) 435–450.
[48] P.J. Linstrom, W.G. Mallard, The NIST Chemistry WebBook: a chemical data resource on the internet, J.Chem.Eng.Data 46 (5) (2001) 1059–1063.
[49] C.S. Land, Calculation of imbibition relative permeability for two and three-phase flow from rock properties, Soc. Pet. Eng. J. 8 (2) (1968) 149. &amp.
[50] F. Riis, E. Halland, CO2 storage atlas of the Norwegian continental shelf: methods used to evaluate capacity and maturity of the CO2 storage potential, Energy Procedia 63 (2014) 5258–5265.
[51] T. Bai, P. Tahmasebi, Coupled hydro-mechanical analysis of seasonal underground hydrogen storage in a saline aquifer, J.Energy Storage (2022) 50.